https://doi.org/10.26599/FRICT.2026.9441341

Research Article

Role of tribolayers in fretting wear in temperature cycling

Yulei Yang[1], Chunshuai Dong[1], Chunhui Gao[2,✉], Haiyu Wang[1], Haiyue Ren[1], Yi Liang[1]

[1] School of Mechanical Engineering, Nanjing University of Science and Technology, Nanjing, 210094, China.

[2] Beijing Power Machinery Research Institute, Beijing, 100074, China.

✉ Corresponding author. E-mail: dzjdchunhui@126.com

Received: August 4, 2026; Revised: October 30, 2026; Accepted: November 18, 2026

© The Author(s) 2026.

Just Accepted

Abstract: The role of tribolayers in fretting wear is well understood under isothermal conditions. However, their effects under temperature cycling remain to be elucidated. In the present study, the role of tribolayers in temperature-cycling fretting wear was investigated. Fretting tests were conducted at room temperature (RT, 25 °C), 750 °C (HT), and RT-to-750 °C cycling (TC) conditions. Systematic tribological analyses were performed to characterize the wear scars and tribolayers. The results show that the formation of coherent tribo-sintered tribolayers resulted in a remarkable reduction in both the friction coefficient and the wear rate as the temperature increased from RT to

750 °C. Thermal cycling led to the formation of concentrated cracks and subsequent localized delamination of the coating. Compacted-debris tribolayers formed at RT transformed into tribo-sintered tribolayers during the subsequent HT stage. These tribo-sintered tribolayers were susceptible to cracking and delamination due to their brittleness in the following RT stage. Despite these detrimental effects, the tribolayers maintained relatively high coverage on the wear scar and remained effective in reducing the wear rate under TC conditions.

Keywords: Tribolayer; fretting wear; temperature cycling; NiCrAlY coating

1 Introduction

Fretting wear refers to the removal of material resulting from small-displacement oscillatory motions, typically excited by mechanical vibrations. It poses a threat to many industrial applications, including dovetail joints in aeroengines [1,2], orthopedic prostheses [3,4], and nuclear fuel assemblies [5]. A clear understanding of friction and wear responses, as well as the associated mechanisms under fretting conditions, is of great significance for ensuring the safe operation of various engineering systems.

Besides the inherent response of the contacting surfaces to the operational parameters, another key factor governing the tribological performance under fretting conditions is the behavior of the wear debris. Owing to the small displacement, the removal of wear debris is much more difficult in fretting than that in sliding [6]. The retained debris may act as third-body particles, or be compacted and even tribo-sintered to form tribolayers. It is widely recognized that the tribo-sintered tribolayers formed at elevated temperatures exhibit superior friction-reducing and anti-wear capabilities [7,8]. In contrast, the compacted-debris tribolayers are prone to cracking and fracture, rendering them incapable of effectively reducing friction and wear [9,10]. Temperature serves as the primary driving force for the microstructural and property evolution of tribolayers: high temperatures

Just Accepted

facilitate the generation of coherently tribo-sintered tribolayers by accelerating the diffusion process, while lower temperatures favor the formation of compacted-debris tribolayers as a result of the limited diffusion process [8,11,12]. Dreano [13] revealed that the oxidized hard debris tribolayers increased the wear volume of a cobalt alloy by four times and the fluctuation in the friction coefficients as the temperature increased from room temperature (RT) to 150 °C. Hager [14] showed that well tribo-sintered tribolayers were formed at 300 °C for a titanium alloy, which resulted in the remarkable reduction of friction coefficient from 0.83 to 0.35, and a substantial decrease in the wear rate. Yang [8] further reported that rising temperatures promotes the coverage of tribo-sintered tribolayers substantially and could lead to a 98.5% reduction in the wear rate of a TiAl alloy at 750 °C compared with that at RT.

While previous studies have clarified fretting properties under isothermal conditions, the role of tribolayers in friction and wear during temperature cycling has received less attention. Glascott [15] and Koricherla [16] observed that thermal stresses induced by temperature cycling did not induce cracking or delamination of the tribolayers formed at high temperature (HT), whereas subsequent RT fretting caused their rapid degradation. The ineffectiveness of tribolayers in reducing friction and wear was ascribed to their instability under normal load and friction force at RT. In contrast, further investigation by Fouvry [17] proved that despite more severe wear of the tribolayers formed at HT during RT fretting, they remained effective in lowering wear volume compared with RT tests. Fouvry found that the tribolayers can withstand RT fretting wear, and even after being damaged, the resulting debris tends to agglomerate and thereby decreases wear volume.

The above studies have laid a foundation for understanding fretting wear under temperature cycling, yet two fundamental questions remain open. One concerns the structural changes of tribolayers when they are generated at one temperature and subsequently fretted at the other; the other is the extent to which the tribolayers formed at HT is damaged during the subsequent RT fretting. To address the issues, both RT-to-HT and HT-to-RT tests were performed to clarify the

Just Accepted

structural changes of tribolayers subjected to varying thermal conditions, and quantitative characterization of tribolayer coverage was conducted to quantify the extent of tribolayer destruction. A NiCrAlY coating was utilized to conducted the fretting wear tests. The coating investigated herein is a promising candidate for the wear-resistance applications in the dovetail connections of aeroengines, which experience RT-to-HT cycling fretting during the startup-operation-shutdown service cycles. Such temperature cycling makes this coating particularly relevant for evaluating the role of tribolayers.

2 Experimental methods

2.1 Materials of samples

NiCrAlY powders with the nominal composition of Ni-23.0%Cr-6.0%Al-0.5%Y (supplied by JIORIE thermal spray materials Ltd.) were used to prepare the coatings. The particle distribution ranges mainly from 45 μm to 83 μm, with a mean particle size D_{50} of 65 μm. High-Velocity Oxygen-Fuel (HVOF) spraying was utilized to spray the NiCrAlY coating to a thickness of 250 μm, and the spraying parameters are listed in Table 1. The substrate were disks with the diameter of 24.0 mm and the thickness of 7.9 mm made of the GH4169 alloy. After spraying, the coatings were mechanically ground to the surface roughness of R*a* 1.2 μm.

Table 1 Plasma spray parameters

Oxygen flow rate (L/min)	Fuel flow rate (L/h)	Standoff distance (mm)	Traverse speed (mm/s)	Powder feed rate (g/min)
100	5.7	320	250	3.5

The counterpart material was a nickel-based superalloy with the nominal composition of Ni-16.0%Cr-13.0%Co-4.0%W-4.0%Mo-3.7%Ti-1.0%Fe-0.7%Nb (supplied by Central Iron & Steel Research Institute of China). The counterpart was machined to the diameter of 10.3 mm with the surface roughness of Ra 1.0 μm. All the samples were ultrasonically cleaned using acetone and ethanol (15 min in each) before the fretting tests.

Just Accepted

2.2 Fretting tests

A reciprocating tribometer (SRV-IV, Optimal Co., LTD) was utilized to perform the fretting tests. The coatings and the counterparts were used as the lower and upper samples, respectively. The fretting stroke of 50 μm with a reciprocating frequency of 20 Hz under a 5 N normal load was adopted. The normal load was chosen to yield an average contact pressure of 468 MPa, which corresponded to the contact pressure of a dovetail connection. The fretting stroke and frequency were chosen based on previous literatures [2,10,11]. The tests were conducted at room temperature (RT, 25 °C), 750 °C (HT), and RT-to-750 °C cycling (TC). The RT and HT tests each lasted 1 h. The TC test consisted of three 20-min cycles, giving a total fretting duration of 1 h. Three repeated tests were carried out at each test condition and the averaged wear rates were presented in the following sections.

2.3 Characterization methods

The crystalline structures of the sprayed NiCrAlY coating were studied with X-ray Diffraction (XRD) (D8 Advance, Bruker) with monochromatic Cu Kα radiation with a wavelength of 0.15406 nm. The measurement range was 10-80° and the step size was 0.02°. A three-dimensional white-light interfering profilometer (Nexview, ZYGO) was used to measure the wear volumes of the samples. Before measuring, the samples were cleaned with ethanol for 5 min ultrasonically to remove the loose debris. The wear scars, debris, and tribolayers were analyzed using a scanning electron microscope (SEM) (JSM-IT500HR, JEOL) equipped with an energy dispersive spectrometer (EDS) (Xplore, Oxford). X-ray Photoelectron Spectroscopy (XPS) (Quantum 2000, PHI) with a monochromatic Al Kα X-ray source was used to specify the chemical state of the elements in the wear scars.

Transmission electron microscope (TEM) (Tecnai G2F30, FEI) characterization of the tribolayers was performed at an accelerating voltage of 300 kV. Focused ion beam milling (FIB) was used to

Just Accepted

extract the TEM lamellas. Nanohardness of the tribolayers and the NiCrAlY coatings were investigated using a high-temperature nanoindenter (TI990, Bruker) at both RT and 750 °C. The maximum test load and loading rate were 1 mN and 2 mN/min, respectively. A 2 s holding time was applied to guarantee the reliability of the obtained elastic modulus. Five independent indentation tests were conducted under each condition, and the average nanohardness and elastic modulus were reported.

3 Results

3.1 Coating characterization

SEM and XRD analyses were carried out to characterize the sprayed NiCrAlY coating, and the corresponding results are presented in Fig. 1. Parallel grooves produced by the mechanical milling were observed on the coating surface (Fig. 1a). The EDS results indicated that, as a consequence of oxidation during the spraying process, the coating was slightly oxidized. The XRD pattern shown in Fig. 1b reveals that the coating was primarily composed of γ-Ni(Cr) and γ′-Ni_3Al phases.

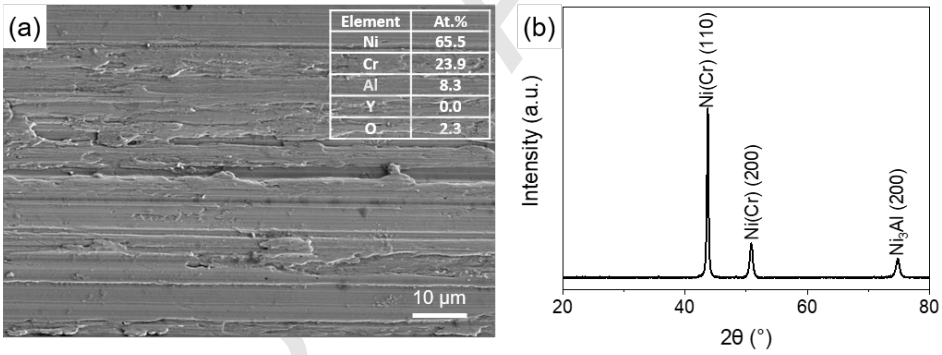


Fig. 1 SEM and XRD characterization of NiCrAlY coating: (a) SEM surface morphology and composition of coating; (b) XRD pattern identifying main crystalline phases.

3.2 Fretting behaviors

The evolution of friction coefficients in both RT and HT is exhibited in Fig. 2. As shown in Fig. 2a, the friction coefficient for the RT test fluctuated between 1.30 and 1.64 during the initial 200 s.

Subsequently, it increased and stabilized at approximately 1.67. In contrast, the friction coefficient exhibited a markedly different pattern at HT. It declined sharply from 1.78 to 0.93 within the first 260 s, and then decreased gradually to 0.84 at 1200 s, after which it remained stable. The friction coefficient versus displacement curves are shown in Fig. 2b. The sliding ratio criteria from Fouvry [18] can be used for quantitative determination of fretting regimes. The sliding ratio, *D,* equals the displacement at zero tangential force, δ_0, divided by the nominal fretting amplitude, δ, and values above 0.26 indicate the gross slip regime. The obtained sliding ratios were 0.94 and 0.86 for the RT and HT tests respectively. Therefore, it can be concluded that both the RT and HT fretting tests operated in the gross slip regime.

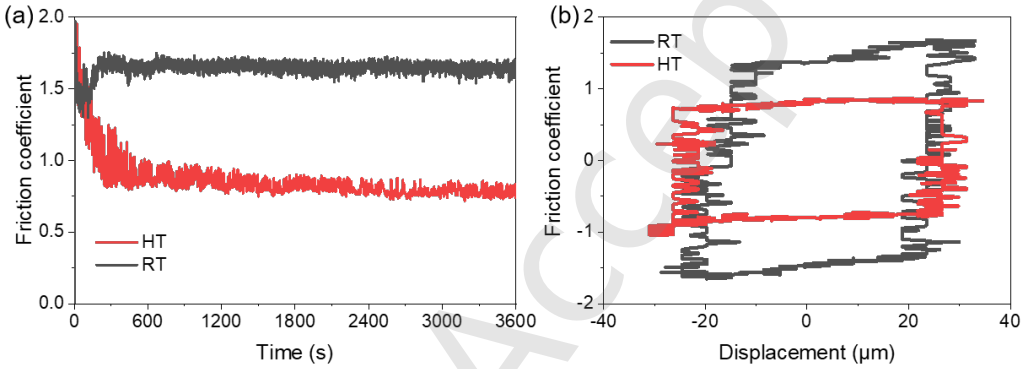


Fig. 2 Evolution of friction coefficient under RT and HT conditions: (a) variation of friction coefficient with fretting cycles at RT and HT; (b) friction coefficient versus displacement (i.e., friction-displacement hysteresis loops) at steady-state stage for RT and HT.

Fig. 3 illustrates the evolution of friction coefficient for the temperature cycling (TC) test. Initially, during the first RT stage, the coefficient exhibited behavior similar to that of the RT test, eventually leveled off at around 1.67. Upon heating to 750 °C, the friction coefficient dropped sharply over the first 200 s and then stabilized at approximately 0.82. In subsequent cycles, the friction coefficient followed a similar pattern to that of the first cycle, along with a slight decrease during the HT stages. Fig. 3b shows the friction coefficient-displacement loops for the temperature cycling test. The sliding ratios were 0.77 and 0.88 for the RT and HT stages respectively, indicating the TC test was in the gross slip regime as well.

Just Accepted

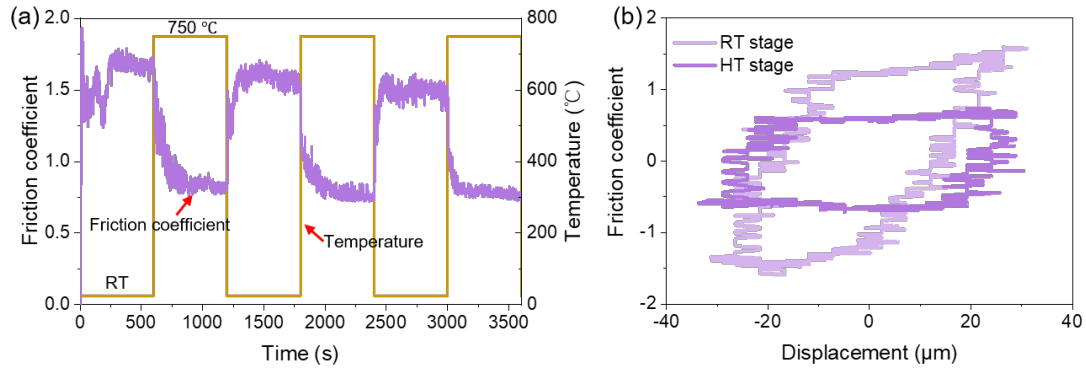
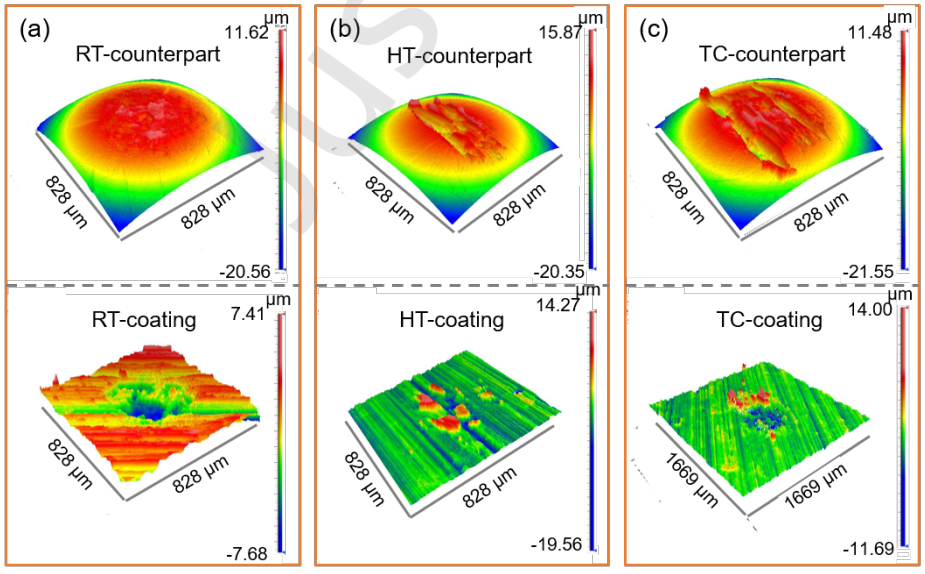


Fig. 3 Friction coefficient evolution under temperature cycling (TC) fretting condition: (a) variation of friction coefficient with fretting cycles; (b) friction coefficient versus displacement at RT and HT stages in steady-state period.

Fig. 4 presents the three-dimensional wear scar morphology for the NiCrAlY coatings and the counterparts. As shown in Fig. 4a, a clear wear pit can be observed on the NiCrAlY coating in the RT test, while the wear of the counterpart was relatively mild. In contrast, the HT test produced different wear scars (Fig. 4b). Severe abrasive grooves and material accumulation were identified on the counterpart. However, the wear on the NiCrAlY coating was slight, and evident material transfer was found on the coating surface. The wear scar of the counterpart in the TC test was similar to that in the HT test, as shown in Fig. 4c. Both wear pits and adhesive material transfer were evident on the NiCrAlY coating surface.



Just Accepted

Fig. 4 Three-dimensional white-light interferometry images of wear scars on NiCrAlY coating and corresponding counterpart balls for fretting tests under different temperature conditions: (a) RT test, (b) HT test, (c) TC test.

A comparison of the wear rates of the NiCrAlY coating and the counterpart ball is presented in Fig. 5. As shown in Fig. 5a, the wear rate of the NiCrAlY coating was 1.90×10^{-5} $mm^3/(N\cdot m)$ in the RT test, which decreased remarkably by 94.8% to 9.96×10^{-7} $mm^3/(N\cdot m)$ in the HT test. For the TC test, an intermediate wear rate of 8.89×10^{-6} $mm^3/(N\cdot m)$ was obtained, which was 53.2% lower than that of the RT test. Fig. 5b reveals that the wear rate of the counterpart ball exhibited a different trend. The wear rate was 9.26×10^{-6} $mm^3/(N\cdot m)$ in the RT test, which increased evidently to 1.55×10^{-5} $mm^3/(N\cdot m)$ and 2.12×10^{-5} $mm^3/(N\cdot m)$ for the HT and TC tests, respectively.

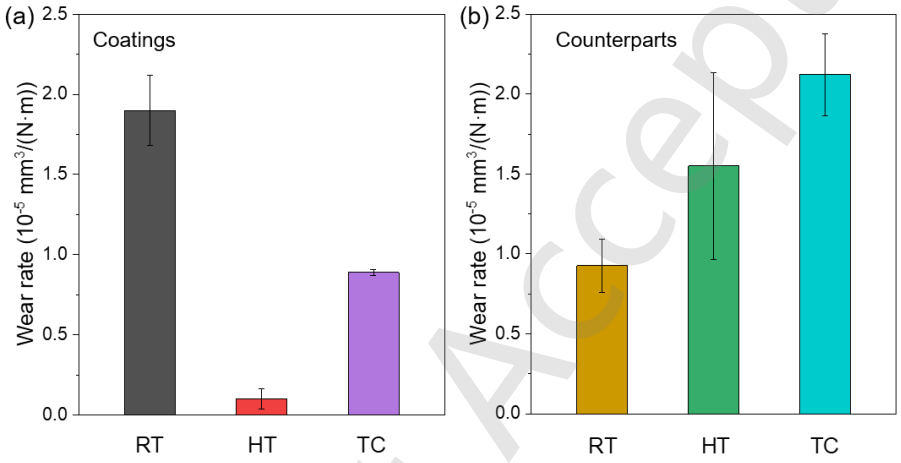


Fig. 5 Wear rates of NiCrAlY coatings and counterpart balls for fretting tests at RT, HT, and TC: (a) wear rates of coating; (b) wear rates of counterpart ball.

3.3 Wear scar analysis

To elucidate wear mechanisms and the role of tribolayers in temperature cycling, the wear scars were investigated with SEM, EDS and XPS. Fig. 6 presents the wear scar morphology of the NiCrAlY coating and the counterpart produced by the RT test. As shown in Figs. 6a and b, despite the parallel grooves induced by abrasive wear, surface cracks and delamination pits were found in the wear scar of the NiCrAlY coating. Owing to the difficulty in ejecting debris during fretting, the wear debris was retained in the wear scar and agglomerated into tribolayers by subsequent fretting (Fig. 6c). As

Just Accepted

reported by previous studies [8,10], the tribolayers formed by the agglomeration and compaction of wear debris, where the individual particles are distinguishable, can be defined as compacted-debris tribolayers. In contrast, the tribolayers developed by tribo-sintering the debris into a solid layer, where individual particles are indistinguishable, can be classified as tribo-sintered tribolayers. According to this classification, the tribolayers in Fig. 6c and f can be attributed to compacted-debris tribolayers. As previously reported, the low diffusion at RT results in insufficient tribo-sintering among the debris, and the tribolayer is prone to form cracks[8,13]. In this study, the cracks in Fig. 6c evidenced the above findings. The wear debris was predominantly micrometer- and sub-micrometer-sized as demonstrated in Fig. 6d. EDS analysis further revealed that the debris was heavily oxidized, with an oxygen content of 50.6 at. %, along with minor amounts of Co, Ti, and W originating from the nickel counterpart. The wear scar morphology of the counterpart ball resembled that of the NiCrAlY coating as shown in Figs. 6e and f, where abrasive wear grooves, delamination induced by surface cracks, and accumulated tribolayer were clearly observed.

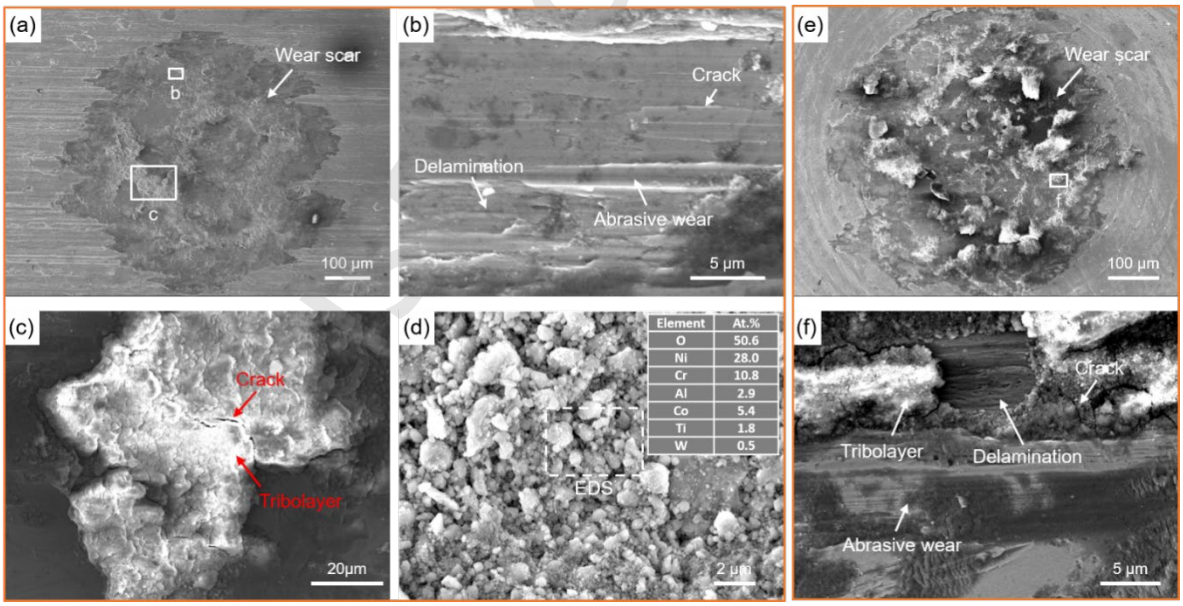


Fig. 6 SEM images of wear scars and debris for RT fretting test: (a) overall morphology of wear scar on NiCrAlY coating; (b) magnified view of region b in (a); (c) magnified view of region c in (a); (d) morphology and composition of wear debris on coating surface; (e) overall morphology of wear scar on counterpart ball; (f) magnified view of region f in (e).

As exhibited in Fig. 7, a remarkably different wear scar from that in the RT test was produced by the HT test. Most of the wear scar was covered by tribolayers ranging from tens to hundreds of micrometers in size (Fig. 7a). In areas without tribolayers, mild parallel grooves generated by abrasive wear were observed (Fig. 7b). The wear debris was predominantly tens to hundreds of nanometers in size, as shown in Fig. 7c, which was much smaller than that of the debris in the RT test. EDS analysis showed that, aside from a slightly higher oxygen concentration, the debris composition was similar to that found in the RT test. A magnified image (Fig. 7d) shows that the tribolayer was coherently tribo-sintered, with individual debris particles being indiscernible. The abrasive wear grooves indicated the occurrence of abrasive wear on the tribolayers. Further EDS examination revealed that the tribolayers had a composition resembling that of the wear debris, and the slightly higher oxygen enrichment could be attributed to the tribo-oxidation during fretting. As shown in Fig. 7e, large areas of tribolayers and pits formed by adhesive transfer were observed on the counterpart. The magnified image in Fig. 7f showed that tribolayers were prone to form cracks, which further developed into tribolayer delamination and fracture.

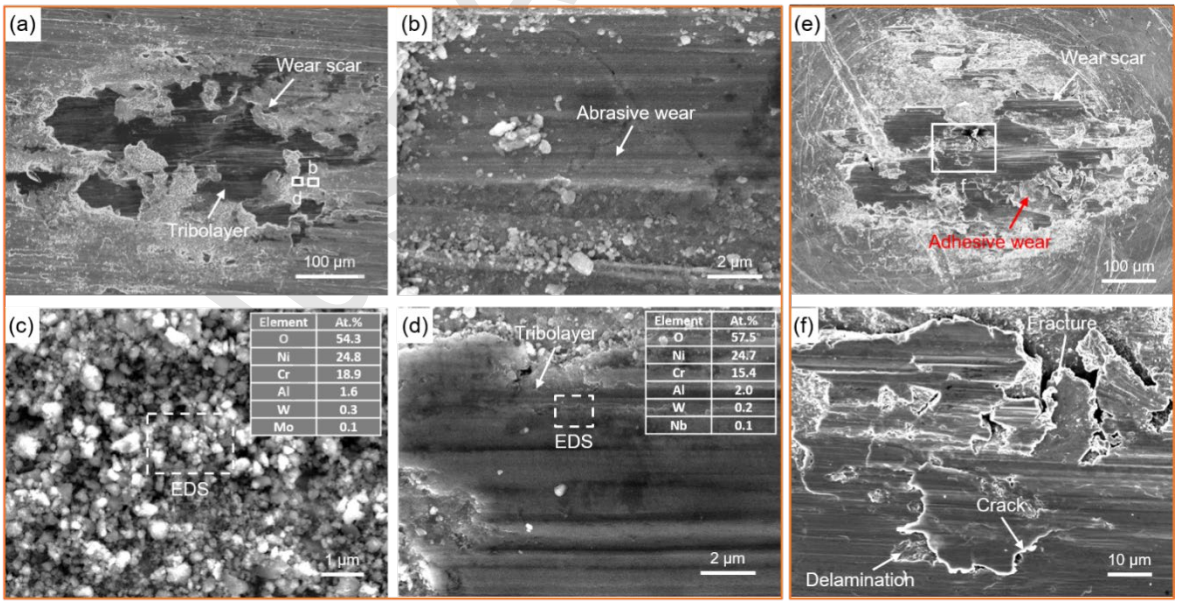


Fig. 7 SEM images of wear scars and debris for HT fretting test: (a) overall morphology of wear scar on NiCrAlY coating; (b) magnified view of region b in (a); (c) morphology and distribution of wear debris on coating surface; (d)

Accepted

magnified view of region d in (a); (e) overall morphology of wear scar on counterpart ball; (f) magnified view of region f in (e).

Fig. 8 illustrates the wear scars produced by the TC test. Figs. 8a and b show that the NiCrAlY coating suffered abrasive wear and delamination, similar to that observed in the RT and HT tests. In contrast, Figs. 8c and d reveal a wear mechanism different from that in the RT and HT tests. The EDS results indicated that the NiCrAlY coating was oxidized during fretting, with an oxygen content of 9.1 at.%. A high density of localized cracks and local delamination was observed on the coating surface (Fig. 8c). FIB milling was performed along the orange line marked in Fig. 8c and the result is shown in Fig. 8d. The cross-sectional analysis revealed that subsurface cracks parallel to the surface had developed, which could lead to local delamination of the coating. Fig. 8e shows the surface morphology of the tribolayers, where cracks and local fractures were observed. The cross-sectional view in Fig. 8f further reveals that subsurface cracks were also produced within the tribolayer. On the counterpart surface (Fig. 8g), extensive abrasive wear grooves and a number of pits produced by adhesive transfer can be observed. Moreover, the tribolayers on the counterpart also exhibited severe cracking and delamination (Fig. 8h), consistent with those observed in the tribolayers on the NiCrAlY coating surface.

Just Accepted

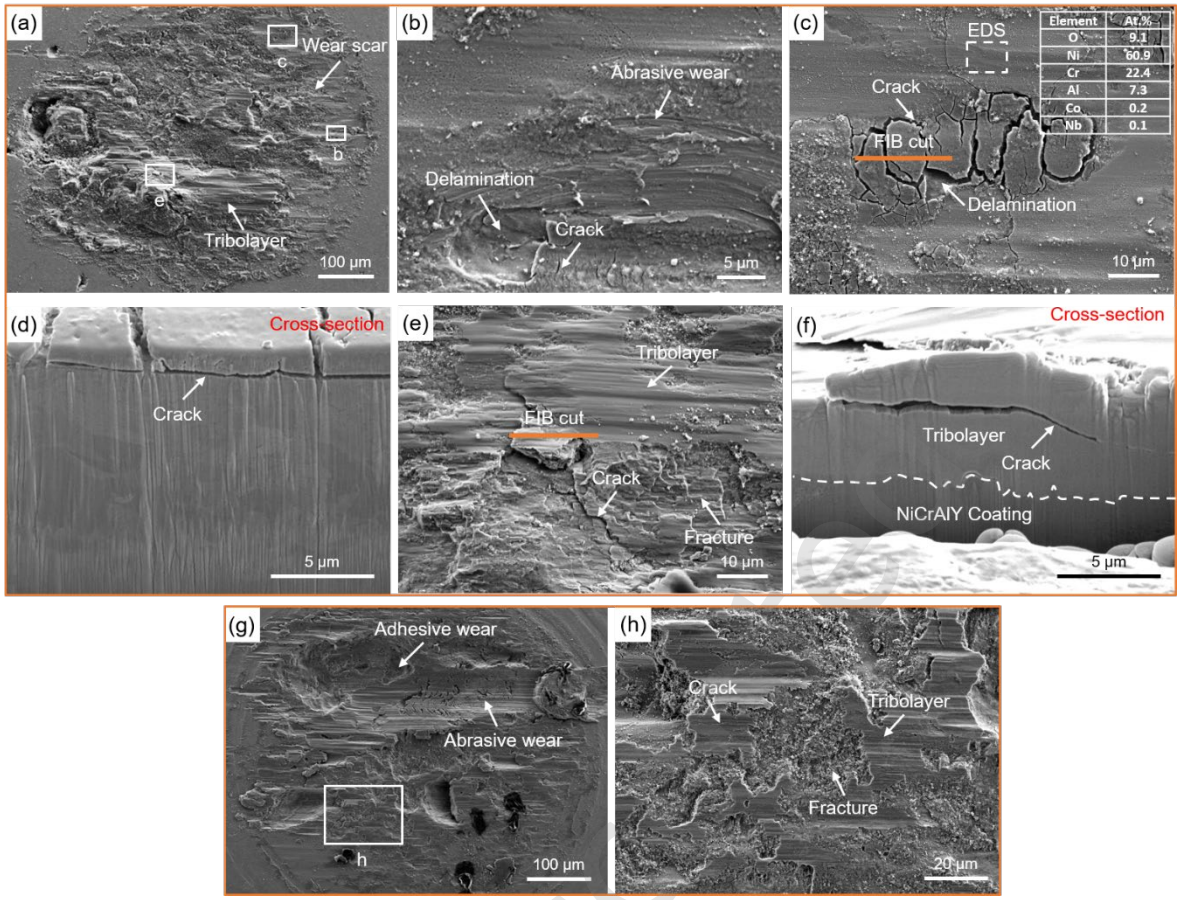


Fig. 8 SEM images of wear scars, debris, and cross-sections for TC fretting test: (a) overall morphology of wear scar on NiCrAlY coating; (b) magnified view of region b in (a); (c) magnified view of region c in (a); (d) cross-sectional morphology along the marked line in (c); (e) magnified view of region e in (a); (f) cross-sectional morphology along the marked line in (e); (g) overall morphology of wear scar on counterpart ball; (h) magnified view of region h in (g).

XPS examination was performed to determine the chemical states of the elements present on the as-sprayed coating and the worn surfaces, and the corresponding full-survey and high-resolution spectra are displayed in Fig. 9. Fig. 9a-1 shows the full-survey spectra for the as-sprayed coating, in which Ni, Cr, Al, Y, and O were detected. The presence of oxygen was due to the oxidation during the spraying process. Figs. 9b-1 to d-1 demonstrate the full-survey spectra for the worn surfaces formed by the RT, HT, and TC tests. In addition to the elements from the NiCrAlY coating, elements originating from the counterpart ball were also detected. The oxygen intensity on the worn surfaces was higher than that of the as-sprayed coating, indicating the occurrence of tribo-oxidation.

Just Accepted

Fig. 9a-2 presents the fitted Ni 2p spectra of the as-sprayed coating. The spectra can be deconvoluted into two distinct components, corresponding to metallic Ni and NiO. Specifically, the peaks centered at 852.7 eV (Ni $2p_{3/2}$) and 869.7 eV (Ni $2p_{1/2}$) are assigned to Ni-Ni metallic bond, with associated satellite peaks observed at 858.6 eV and 875.9 eV, respectively [19,20]. The doublet located at 853.3 eV (Ni $2p_{3/2}$) and 870.9 eV (Ni $2p_{1/2}$) is characteristic of Ni^{2+} in NiO, accompanied by satellite peaks at around 860.8 eV and 878.0 eV. Fig. 9b-2 shows the fitted Ni 2p spectra of the worn surfaces formed by the RT test. Apart from peaks for the metallic Ni and NiO, peaks characteristic of $NiCr_2O_4$ spinel can be clearly identified. The features at 855.8 eV (Ni $2p_{3/2}$) and 873.7 eV (Ni $2p_{1/2}$) correspond to Ni^{2+} in $NiCr_2O_4$ spinel phase, along with satellite peaks at around 862.0 eV and 880.4 eV. As shown in Fig. 9c-2, the Ni 2p spectra acquired from the worn surfaces formed by the HT test closely resembled those from the RT test. Metallic Ni, NiO oxide, and $NiCr_2O_4$ spinel were identified, and their contents were comparable to those observed at RT. For the TC test, although the spectra (Fig. 9d-2) also comprised metallic Ni, NiO oxide, and $NiCr_2O_4$ spinel, the proportion of NiO decreased markedly, whereas that of $NiCr_2O_4$ increased substantially.

Fig. 9a-3 reports the fitted Cr 2p spectra acquired from the as-sprayed coating. The fitted peaks located at 573.9 eV (Cr $2p_{3/2}$) and 583.0 eV (Cr $2p_{1/2}$) are assigned to Cr-Cr metallic bond, whereas those centered at 576.8 eV (Cr $2p_{3/2}$) and 586.4 eV (Cr $2p_{1/2}$) are characteristic of Cr^{3+} in both Cr_2O_3 and $NiCr_2O_4$ spinel [19,20]. The fitted Cr 2p spectra of the worn surfaces formed by the RT test are presented in Fig. 9b-3. The peaks representing Cr-Cr metallic bond reduced significantly, whereas the peaks corresponding to Cr_2O_3 and $NiCr_2O_4$ spinel intensified remarkably, indicating the predominant oxidation of chromium even by the RT test. For the worn surfaces formed by the HT test (Fig. 9c-3), the peaks corresponding to Cr-Cr metallic bond disappear completely, leaving only the peaks attributable to Cr_2O_3 and $NiCr_2O_4$ spinel. As presented in Fig. 9d-3, the spectra produced by the TC test closely resemble those from the HT test, exhibiting exclusively the features of Cr_2O_3 and $NiCr_2O_4$ spinel.

Just Accepted

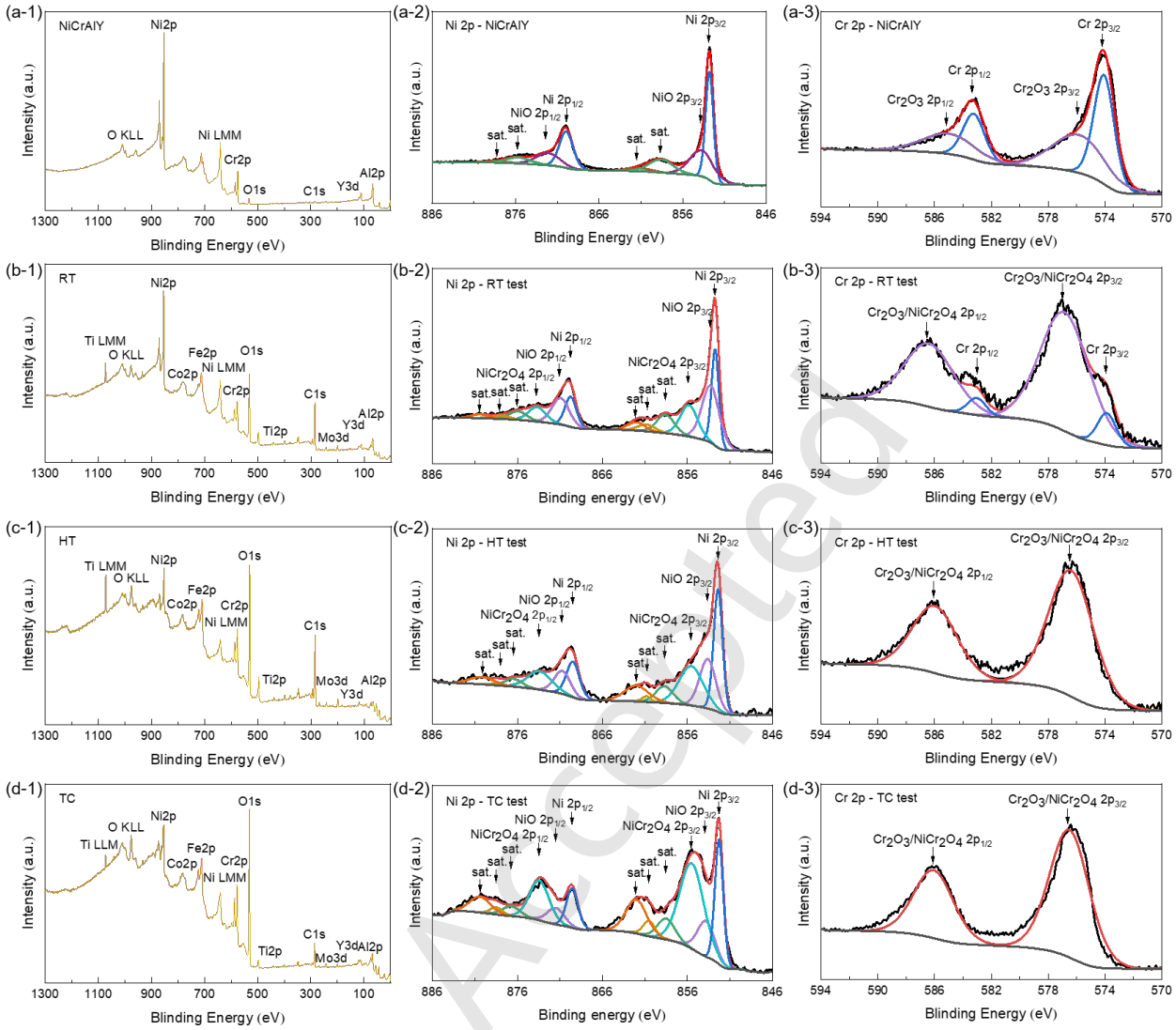


Fig. 9 XPS spectra of as-sprayed coating and worn surfaces formed by RT, HT, and TC fretting tests: (a-1) full-survey spectra of as-sprayed coating; (a-2) Ni 2p spectra of as-sprayed coating; (a-3) Cr 2p spectra of as-sprayed coating; (b-1) full-survey spectra of RT test; (b-2) Ni 2p spectra of RT test; (b-3) Cr 2p spectra of RT test; (c-1) full-survey spectra of HT test; (c-2) Ni 2p spectra of HT test; (c-3) Cr 2p spectra of HT test; (d-1) full-survey spectra of TC test; (d-2) Ni 2p spectra of TC test; (d-3) Cr 2p spectra of TC test.

3.4 Microstructure of tribolayers

TEM analysis was carried out so as to elucidate the microstructure of the tribo-sintered tribolayers. Fig. 10 presents the results of the tribolayer formed during the HT test. As shown in Fig. 10a, the tribolayer had a thickness exceeding 6 μm and exhibited a homogeneous microstructure that was

Just Accepted

virtually free of defects such as voids and cracks. The elemental distribution in Fig. 10b indicates that the tribolayer consisted primarily of Ni, Cr, Al, along with notable oxygen enrichment, in agreement with the EDS analysis of the wear scars (Fig. 7d). Fig. 10c shows that the tribolayers were composed of grains with sizes of tens of nanometers, and the selected-area electron diffraction (SAED) pattern suggests that these nanograins were randomly oriented. It should be noted that SAED patterns alone cannot provide definitive evidence for phase identification because of the overlap among multiple diffraction rings. Therefore, the phases were identified by combining the SAED diffraction rings with the XPS results presented in Fig. 9. Figs. 10d and e demonstrate high-resolution images and Inverse Fast Fourier Transform (IFFT) of several nanograins. The lattice spacings derived from the IFFT pattern confirm the presence of Cr_2O_3, Al_2O_3, NiO, $NiCr_2O_4$ spinel, and unoxidized Ni and NiAl grains, which is consistent with the SAED rings and the XPS analysis (Fig. 9). In addition to the nanograins, Fig. 10f reveals the existence of grains with sizes of around one hundred nanometers in localized regions of the tribolayer. The high-resolution image and Fast Fourier Transform (FFT) spots in Fig. 10g further illustrate the grain microstructure. The lattice spacing of 0.204 nm measured from the IFFT pattern agrees well with the Ni (111) interplanar spacing.

Just Accepted

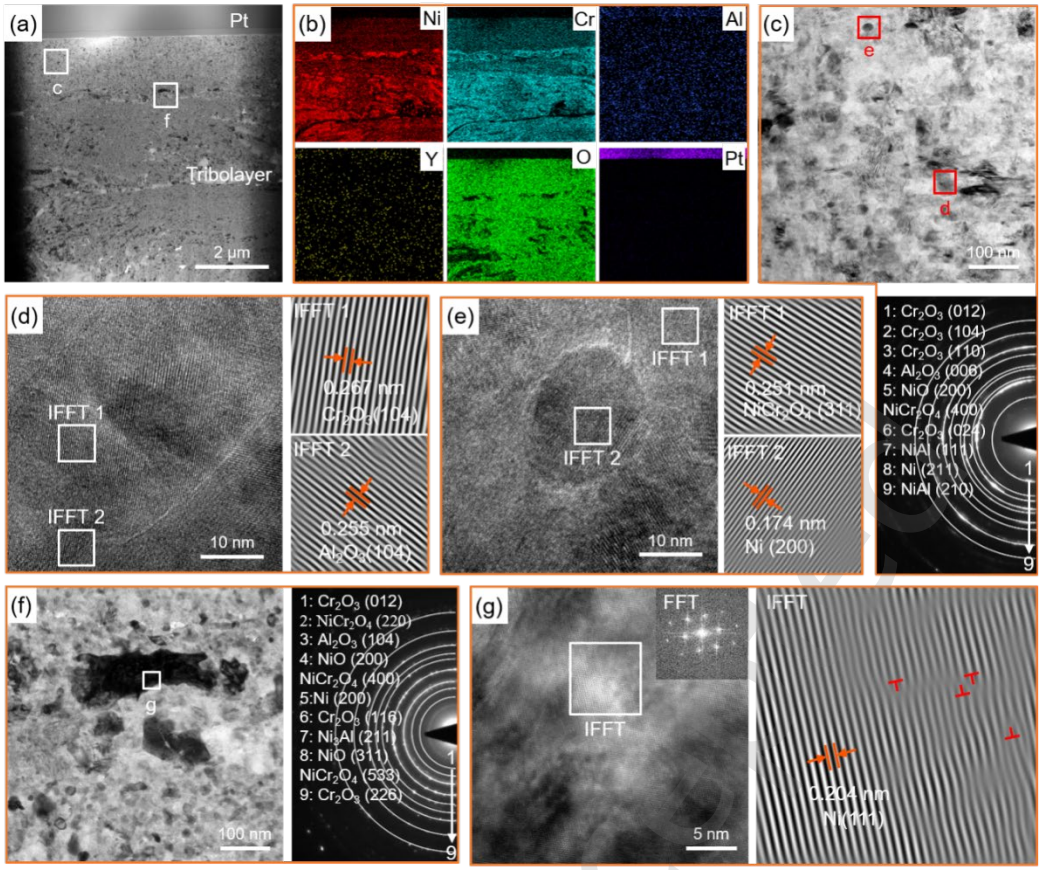


Fig. 10 TEM characterization of tribolayers formed by HT fretting test: (a) low-magnification bright-field TEM image showing overall morphology; (b) corresponding EDS elemental distribution maps; (c) magnified view of region c in (a); (d) high-resolution TEM (HRTEM) image of region d in (c); (e) HRTEM image of region e in (c); (f) magnified view of region f in (a); (g) HRTEM image of region g in (f).

Fig. 11 demonstrates the TEM characterization of the tribolayer produced by the TC test. As shown in Fig. 11a, the tribolayer exhibits a thickness of approximately 0.8-1.1 μm, with some voids observed in the bottom region. The EDS elemental mapping in Fig. 11b indicates that the composition of the tribolayer resembles that formed during the HT test. Moreover, an unoxidized grain, enriched in Ni and measuring several hundred nanometers in size, is clearly discernible in the elemental distribution. The tribolayer was composed of randomly oriented nanograins, including Cr_2O_3, Al_2O_3, NiO, $NiCr_2O_4$ spinel, as well as unoxidized Ni and Ni_3Al, as confirmed by the morphology and SAED rings in Fig. 11c. High-resolution analysis and the corresponding IFFT lattice spacings further reveal the presence of Cr_2O_3 and Al_2O_3 nanograins (Fig. 11d). Fig. 11e

presents the high-resolution image and the corresponding IFFT pattern of the Ni-rich grain highlighted in Fig. 11a and b. The FFT spots and the measured 0.204 nm lattice spacing confirmed this grain was unoxidized metallic nickel.

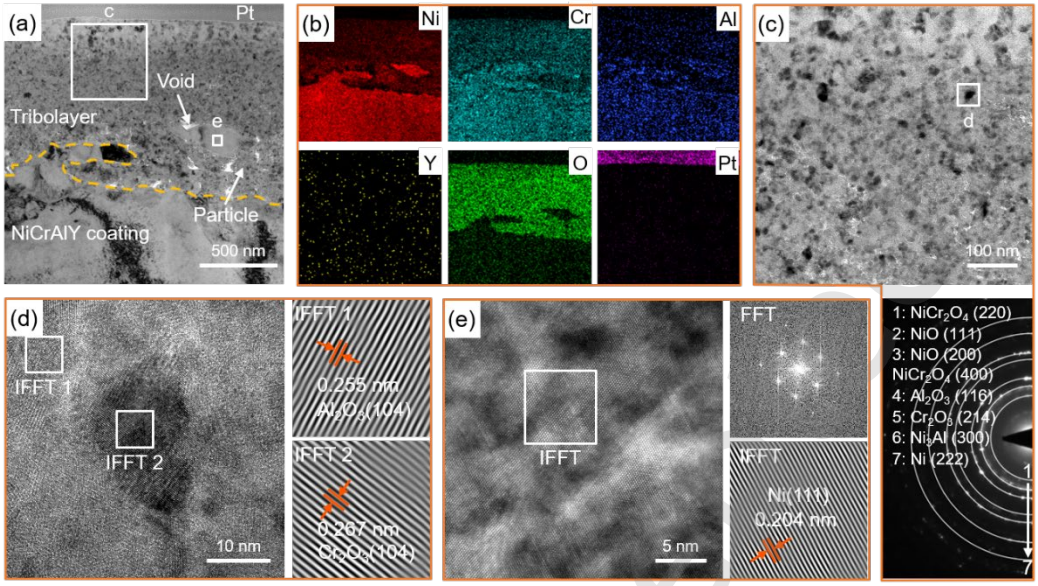


Fig. 11 TEM characterization of tribolayer formed by TC fretting test: (a) low-magnification bright-field TEM image showing overall morphology; (b) corresponding EDS elemental distribution maps; (c) magnified view of region c in (a); (d) HRTEM image of region d in (c); (e) HRTEM image of region e in (a).

3.5 Mechanical properties of tribolayers

To evaluate the mechanical properties of the tribo-sintered tribolayers, nanoindentation tests were conducted at both RT and 750 °C. Fig. 12 compares the indentation depth-load curves, nanohardness, and elastic modulus of the tribolayers with those of the NiCrAlY coating. Fig. 12a presents the experimental setup along with a schematic illustration of the tests. As shown in Fig. 12b, the maximum indentation depths for the tribolayers at RT and HT (750 °C) were 37.7 nm and 51.8 nm, respectively. The NiCrAlY coating, by contrast, exhibited larger maximum indentation depths of 47.2 nm and 64.1 nm under the same temperature conditions. The NiCrAlY coating demonstrated a nanohardness of 7.7 GPa at RT, which decreased substantially by 50.6% to 3.8 GPa at HT (Fig. 12c). Despite this sharp drop in nanohardness, its elastic modulus declined only slightly, from 173.3 GPa

Just Accepted

at RT to 159.5 GPa at HT. Fig. 12d reveals that the tribolayers exhibited a considerably high nanohardness of 20.2 GPa at RT, which also decreased remarkably to 7.4 GPa at HT. The elastic modulus of the tribolayer was 261.4 GPa and 221.3 GPa at RT and HT, respectively. The tribo-sintered tribolayers in the TC samples were formed during the high-temperature stages and have compositions and structures similar to those of the HT tribolayers (Figs. 10 and 11). Therefore, their nanohardness and elastic modulus are therefore expected to be comparable to those of the HT tribolayers.

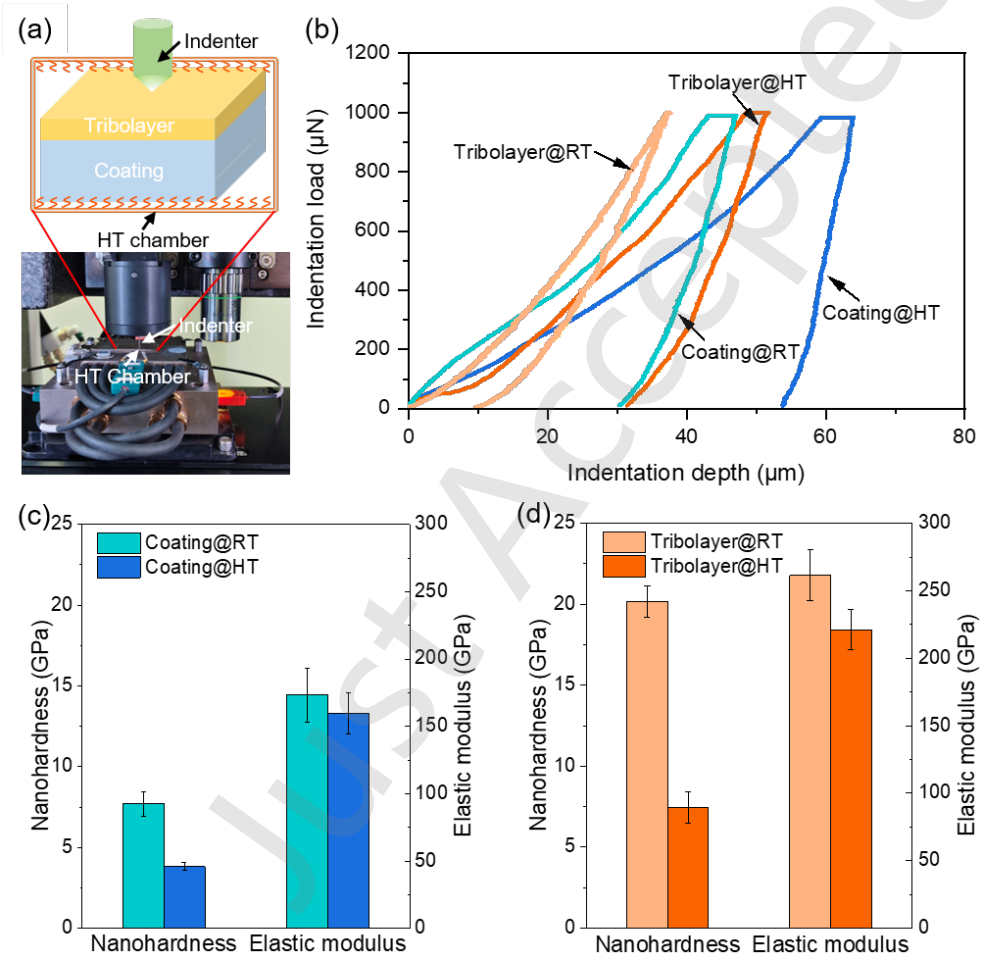


Fig. 12 Nanoindentation characterization of tribolayers and NiCrAlY coating at RT and HT (750 °C) conditions: (a) schematic diagram of experimental setup; (b) representative load–displacement indentation curves; (c) elastic modulus and hardness of NiCrAlY coatings; (d) elastic modulus and hardness of tribolayers.

Just Accepted

4 Discussion

4.1 Role of tribolayers in RT and HT fretting

During RT fretting, the NiCrAlY coating was characterized by crack formation and localized delamination (Fig. 6b). The debris was heavily oxidized and primarily micrometer and sub-micrometer scale (Fig. 6d). The oxidized debris exhibited high hardness at RT, which subsequently resulted in severe abrasive wear of the coating (Fig. 6b). As established previously, the formation of tribolayers in fretting stems from the agglomeration, compaction, and tribo-sintering of wear debris [21,22]. Temperature-driven atomic diffusion plays a key role in the formation of coherently tribo-sintered tribolayers [8,23]. The tribolayers in Fig. 6c displayed a microstructure of compacted debris with insufficient tribo-sintering, rendering them prone to cracking and fracture. The resulting fractured tribolayers and debris further aggravated the wear and elevated the friction coefficient. Ultimately, the combined effects of severe cracking, localized delamination, abrasive wear, and the ineffective protection of tribolayers led to the high friction coefficient (Fig. 2) and wear rate (Fig. 5) of the NiCrAlY coating at RT.

In contrast, the HT test was characterized by the substantial adhesive transfer of the counterpart material to the NiCrAlY coating (Fig. 4b). Most areas of the wear scar on the coating were covered by coherently tribo-sintered tribolayers (Figs. 7a and d). This microstructural transformation of the tribolayers from compacted debris at RT to a dense and homogeneous structure at HT stems primarily from the reduced debris size and the enhanced atomic diffusion. On one hand, the decrease in debris size markedly increases the adhesion strength among debris particles according to the JKR adhesion model, which consequently facilitates the agglomeration and compaction process [24,25]. On the other hand, the diffusion coefficients increase significantly with rising temperature, thereby promoting tribo-sintering and the formation of dense tribolayers with fewer defects [8]. The XPS and TEM analyses presented in Figs. 9 and 10 corroborate the dense and almost defect-free microstructure of tribolayers. The dense nanograined microstructure with few defects in the

Just Accepted

tribolayers indicates improved mechanical properties and wear resistance, corroborated by previous nanoindentation at RT [8,26]. Our results show that, besides the enhanced nanohardness at RT, the tribolayer nanohardness remained 95% higher than that of the NiCrAlY coating even at 750 °C (Fig. 12d). The tribolayers, owing to their excellent wear resistance and extensive coverage on the wear scar, effectively shielded the NiCrAlY coating from exposure and subsequent wear, thus lowering both the friction coefficient and wear rate at HT.

4.2 Role of tribolayers in temperature-cycling fretting

The friction and wear response in temperature-cycling fretting is influenced by both the intrinsic properties of the NiCrAlY coating and the characteristics of the tribolayers. In the following, the coating's contribution will be discussed first.

Adhesive material transfer from the counterpart, abrasive wear, localized cracking and subsequent delamination, resembling those in the RT and HT tests (Figs. 3c, 6b and 7b), were also identified in the TC tests (Fig. 8b). In contrast, the TC tests further revealed locally concentrated cracks and delamination of the coating substrate (Figs. 8c and d). Previous investigations have revealed that temperature cycling brings about aggravated oxidation and cyclic thermal stress induced cracking, which in turn compromise wear resistance [27-29]. Table 2 compares the coefficients of thermal expansion for the oxides and the coating substrate [30-32], revealing a significant mismatch between them. Consequently, both the cyclic thermal stresses and the thermal-expansion mismatch contribute to concentrated crack formation. The aggravated oxidation indicated by the Ni 2p and Cr 2p XPS spectra in Fig. 9, and the concentrated cracks in Fig. 8c for the TC tests are consistent with these earlier findings. The concentrated cracks and ensuing localized delamination led to higher friction coefficient and accelerated wear in the TC tests.

Table 2 Coefficient of thermal expansion for oxides and NiCrAlY (10^{-6} K^{-1}) [30-32]

NiCrAlY	NiO	$NiCr_2O_4$	Cr_2O_3	Al_2O_3
15~20	10	10	11	8~10

Just Accepted

The XPS spectra in Fig. 9 further reveal remarkable tribo-oxidation and a notable alteration in the oxide composition for the TC tests. Compared with the as-sprayed NiCrAlY coating, the intensities of the Ni and Cr oxide peaks were markedly higher on the worn surfaces generated by the RT, HT, and TC tests. These results indicate that Ni and Cr oxides formed through tribo-oxidation during the fretting tests other than the spraying proces. Moreover, the RT and HT tests yielded comparable proportions of NiO, $NiCr_2O_4$, and metallic Ni. At elevated temperatures, Cr_2O_3 and NiO are preferentially formed owing to their lower Gibbs free energies [33]. The produced Cr_2O_3 and NiO spinel exert a lubricating effect and thus contribute to the low friction coefficient observed during the HT stages [33-35].

The TC tests exhibited a marked increase in the $NiCr_2O_4$ spinel fraction, rising from 33.5% (HT) to 55.7% (TC), alongside a conspicuous reduction in NiO from 28.2% to 16.5%. These compositional shifts suggest that the cyclic thermal loading facilitated the solid-state reaction $NiO+Cr_2O_3 \rightarrow NiCr_2O_4$. The subsequent reaction between these oxides to generate $NiCr_2O_4$ spinel is thermodynamically favored by the negative Gibbs free energy change, and is further promoted by the tribo-oxidation at elevated temperatures [33,34]. $NiCr_2O_4$ is generally recognized as a hard spinel-type phase with high thermal stability [36]. Therefore, the incorporation of $NiCr_2O_4$ contributes to the improved hardness of the tribolayers under both RT and 750 °C conditions. This hardness enhancement is consistent with the higher nanohardness measured for the tribo-sintered tribolayers compared with the NiCrAlY coating. The high hardness in oxide phases is often accompanied by a trade-off in toughness. $NiCr_2O_4$ spinel exhibits extremely large elastic anisotropy, which can promote strain localization and microcrack initiation under contact stress [33,36]. This may contribute to the generation of cracks observed in the tribo-sintered tribolayers. It is also widely recognized that spinel oxides such as $NiCr_2O_4$ can provide lubricating and wear-reducing effects [33,34,36]. In this study, a high $NiCr_2O_4$ intensity was detected for the TC tests. Consequently, the

Just Accepted

incorporation of $NiCr_2O_4$ spinel is considered to lower the friction coefficient and the wear rate under TC condition.

Besides the intrinsic properties of the NiCrAlY coating, another key factor governing the fretting behaviors is the response of tribolayers to temperature cycling. In particular, two controlling aspects are involved: first, how the compacted-debris tribolayers formed at RT evolve when the temperature rises to HT; and second, how the coherently tribo-sintered tribolayers formed at HT respond during fretting at RT.

To elucidate the tribolayer response to temperature cycling, two independent tests were carried out, with temperature variations from RT to HT in one case and from HT to RT in the other. The response of tribolayers in these tests is presented in Fig. 13 (with the insets depicting the temperature variations). The RT-formed compacted-debris tribolayers experienced significant tribo-sintering at HT, with individual debris particles no longer distinguishable (Figs. 13a and b). The FIB cross-section analysis in Fig. 13c indicates that some voids and cracks were formed in the lower part of the tribolayer, possibly resulting from the large debris produced at RT. As illustrated in Figs. 13d and e, local cracking and ensuing delamination were observed for the coherently tribo-sintered tribolayers (formed at HT) when fretting at RT. The coherently tribo-sintered tribolayers demonstrated remarkably high nanohardness exceeding 20 GPa when evaluated at RT (Fig. 12c). However, the oxide-rich constitution makes the tribolayers brittle and prone to form cracks at RT. As a result, the fragmented high-hardness debris served as a third body, leading to severe abrasive wear of the NiCrAlY coating (Fig. 13f). Similar cracking and fracture phenomena were also observed in the coherently tribo-sintered tribolayers of the TC tests (Figs. 8e and f), providing additional evidence for the temperature-dependent alteration of tribolayers.

Just Accepted

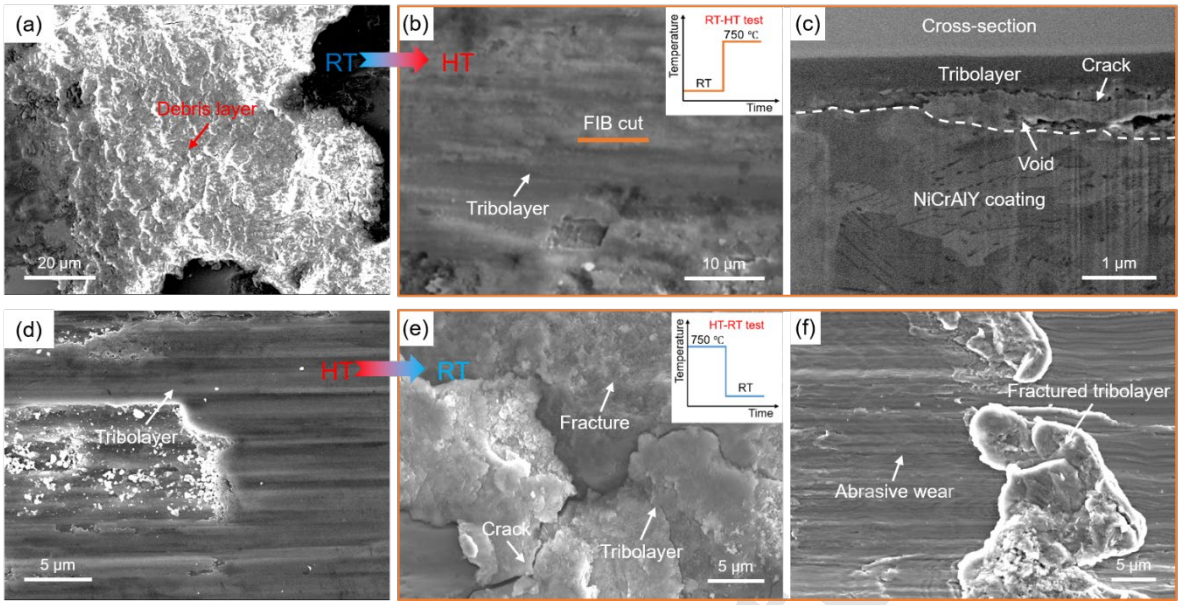


Fig. 13 Evolution of tribolayers under alternating temperature conditions: (a) compacted-debris tribolayer formed during RT stage; (b) highly tribo-sintered tribolayer formed during HT stage; (c) cross-sectional morphology along the marked line in (b); (d) tribolayer formed during HT stage; (e) cracking and fracture of tribolayer during RT stage; (f) abrasive wear induced by tribolayer fragments. The insets indicate the corresponding temperature variations.

Beyond the qualitative discussion above, the areal coverage of tribolayers in the wear scars was quantitatively evaluated with ImageJ, and Fig. 14 presents the comparative results. The compacted-debris tribolayers occupied 12.9% of the scar area in the RT tests. In contrast, the coherently tribo-sintered tribolayers reached 43.3% in the HT tests, representing a substantial increase. For the TC tests, the tribo-sintered tribolayers still exhibited a coverage of 28.3%. As previously established, the friction and wear reduction is strongly related to the coverage of tribo-sintered tribolayers, where a higher coverage generally corresponds to a lower friction coefficient and improved wear resistance [8,36,37]. The high tribolayer coverage was the dominant reason for the low friction coefficient and wear rate observed in the HT tests. In the TC tests, despite the inevitable cracking and fracture of the tribo-sintered tribolayers during the RT stages, the retained coverage was still sufficient to mitigate the wear rate of the NiCrAlY coating.

Just Accepted

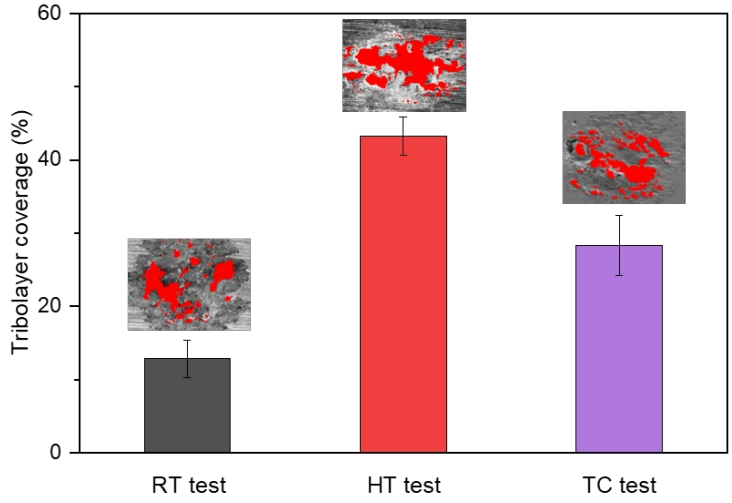


Fig. 14 Areal coverage fraction of tribolayers under RT, HT, and TC fretting conditions.

The quantitative tribolayer coverage analysis further reveals a clear correlation between tribolayer characteristics and the fretting behavior. In the HT tests, the 7.4 GPa nanohardness of tribolayers at 750 °C is approximately 95% higher than that of the NiCrAlY coating (3.8 GPa) at the same temperature, and the 43.3% tribolayer coverage effectively reduced the friction coefficient to 0.84 and the wear rate to 9.96×10^{-7} mm³/(N·m) for the HT tests. This demonstrates the effectiveness of tribo-sintered tribolayers in reducing friction and wear. In contrast, the cracking tendency, and the low coverage of 12.9% made the compacted-debris tribolayers ineffective in alleviating friction and wear, leading to a high friction coefficient of 1.67 and a wear rate of 1.90×10^{-5} mm³/(N·m) in the RT tests. Under TC conditions, the tribolayer coverage was 28.3%, intermediate between those of the RT and HT tests. Correspondingly, the wear rate (8.89×10^{-6} mm³/(N·m)) was 53.2% lower than that of the RT tests but much higher than that of the HT tests. The structural integrity and brittleness of the tribolayers also play critical roles. During the RT stages of TC, the tribo-sintered tribolayers underwent cracking and local delamination, weakening their protective effect. It should be noted that the formation of cracks in the surface tribolayers was different from that in the coating. The formation of cracks in the coating substrate was due to the cyclic thermal stresses and the thermal-expansion mismatch between the oxides and the coating. In contrast, cracks in the surface tribolayers were caused by the brittleness of the oxides at RT and by the microstructural defects such as internal

Just Accepted

voids. Nevertheless, the retained coverage was still sufficient to mitigate coating wear compared with the RT tests. These comparisons confirm that both the coverage and mechanical properties of the tribolayers govern the friction and wear behavior under TC conditions.

The counterpart nickel-based superalloy exhibited markedly higher wear loss under HT and TC conditions than under RT conditions. On the one hand, abrasive wear and the adhesive transfer of the counterpart to the coating were intensified under HT and TC conditions. On the other hand, cracking and local fracture of tribolayers on the counterpart were extensive under both HT and TC conditions (Figs. 7f and 8h), which are likely the consequences of increased spinel oxide content and internal defects in the tribolayers, as well as cyclic thermal stresses. These factors collectively contribute to the increased wear of the counterpart under HT and TC conditions.

Based on the above results and discussion, a schematic illustration summarizing the role of tribolayers in the fretting friction and wear behaviors under temperature cycling is presented in Fig. 15. When fretting at RT, the low diffusion process favored the formation of compacted-debris tribolayers, which were susceptible to cracking and fracture. The resulting low coverage and inadequate protection left the NiCrAlY coating vulnerable to severe abrasive wear, cracking, and delamination, ultimately giving rise to the relatively high friction coefficient and wear rate. In contrast, the rapid diffusion process at HT facilitated the formation of coherently tribo-sintered, nanostructured tribolayers, which provided excellent friction reduction and wear resistance. Owing to their high coverage, only small areas of the NiCrAlY coating were directly exposed to the counterpart, sustaining only mild abrasive wear. As a result, both the friction coefficient and wear rate were significantly reduced. Under temperature-cycling fretting, concentrated cracks and subsequent localized delamination occurred on the NiCrAlY coating. The debris compacted at RT could convert to tribo-sintered tribolayers at the HT stages. Despite cracking and fracture of these sintered layers during later RT stages, their coverage remained relatively high in the wear scar, rendering them effective at lowering the wear rate under temperature cycling conditions.

Just Accepted

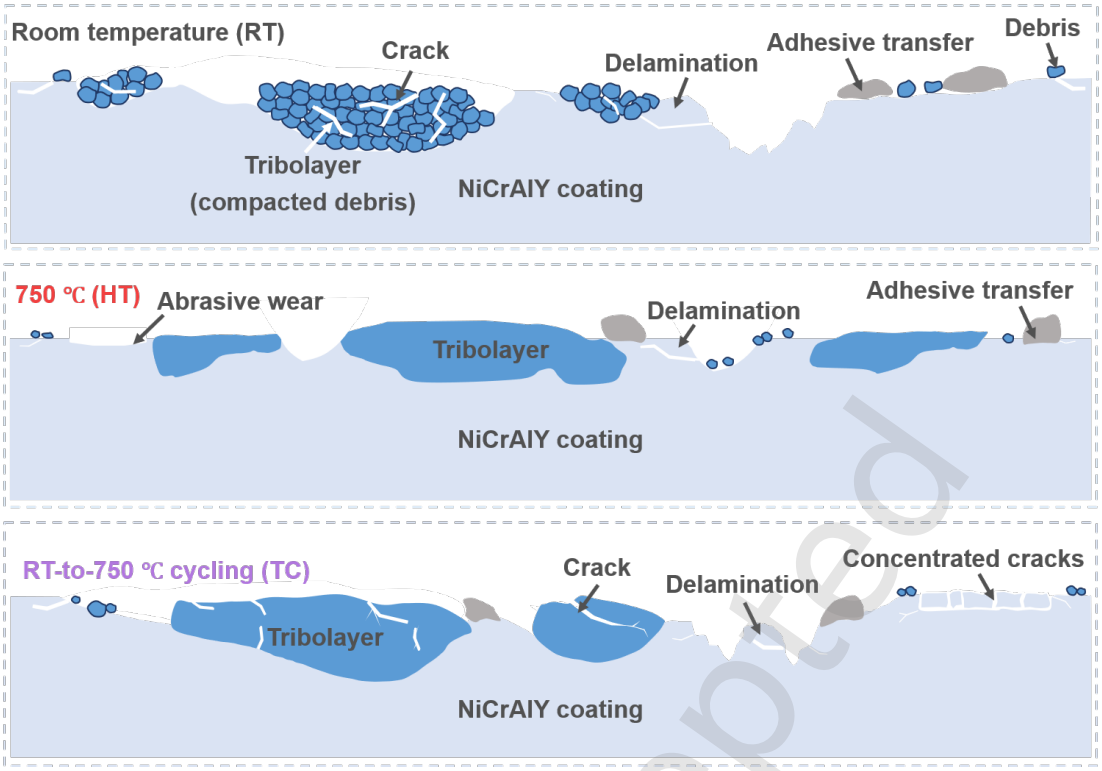


Fig. 15 Schematic illustration of role of tribolayers on friction and wear behaviors in fretting under RT, HT, and TC conditions.

5 Conclusions

In the present study, the role of tribolayers in fretting wear under temperature cycling was investigated. The structural evolution of tribolayers under different thermal conditions was elucidated, and the tribolayer coverage was quantitatively characterized. The following conclusions can be drawn:

1) Tribo-sintered tribolayers exhibit substantially higher nanohardness than the NiCrAlY coating under both RT and HT (750 °C) conditions, which is beneficial for reducing the friction coefficient and wear rate.

2) Compacted-debris tribolayers formed at RT can transform into tribo-sintered tribolayers during the subsequent HT stage. These tribo-sintered tribolayers are prone to cracking and local delamination in the subsequent RT stage owing to their brittleness.

3) Although the tribolayers undergo more severe destruction during the RT stages than during the HT stages, their coverage remains relatively high throughout thermal cycling, making them effective in reducing the wear rate.

Just Accepted

Funding

This research was supported by the National Natural Science Foundation of China (Grant No. 52405200).

Author contributions

Yulei Yang: Writing – review & editing, Writing – original draft, Supervision, Methodology, Investigation, Funding acquisition, Formal analysis, Data curation, Conceptualization. **Chunshuai Dong:** Writing – review & editing, Investigation, Formal analysis, Data curation, Formal analysis. **Chunhui Gao:** Writing – review & editing, Supervision, Formal analysis. **Haiyu Wang:** Writing – review & editing, Investigation, Formal analysis. **Haiyue Ren:** Writing – review & editing, Investigation, Formal analysis. **Yi Liang:** Writing – review & editing, Resources, Investigation, Formal analysis.

Availability of data and materials

Not applicable.

Competing interests

The authors have no competing interests to declare that are relevant to the content of this article.

Just Accepted

References

[1] Chen X J, Han Y F, Xiao K, Li T Y, Fang S. Improving high-temperature fretting wear performance of GTD-450 blade steels via ultrasonic impact treatment-induced Si_3N_4 particle implantation. *J Mater Process Tech*, **342**: 118943 (2025). https://doi.org/10.1016/j.jmatprotec.2025.118943

[2] Yang Y L, Gesang Y Z, Xu J M, Liang Y. Investigation on fretting wear of NiCrAlY coatings at elevated temperature. *Surf Coat Tech*, **459**: 129339 (2023). https://doi.org/10.1016/j.surfcoat.2023.129339

[3] Kim K, Geringer J, Pellier J, Macdonald D. Fretting corrosion damage of total hip prosthesis: friction coefficient and damage rate constant approach. *Tribol Int* **60**: 10-18 (2013). https://doi.org/10.1016/j.triboint.2012.10.008

[4] Zhang T F, Su J, Ke L L. Fretting wear behavior of silicone rubber with biomimetic surface texture. *Friction*, ***13***(8): 9441000 (2025). https://doi.org/10.26599/FRICT.2025.9441000

[5] Chen H, Mei G Y, Chen Y L, Tan W, Zhu G R. Temperature induced wear transition of high-silicon T91 during fretting corrosion in liquid lead-bismuth eutectic. *Tribol Int* **225**: 112415 (2027). https://doi.org/10.1016/j.triboint.2026.112415

[6] Yang Y L, Xu J M, Liang Y. A fretting wear model considering formation of tribolayers. *Ind Lubr Tribol* **75**(4): 372-379 (2023). https://doi.org/10.1108/ILT-01-2023-0001

[7] Everitt N M, Ding J, Bandak G, Shipway P H, Leen S B. Characterisation of fretting-induced wear debris for Ti-6Al-4V. *Wear* **267**: 283-291 (2009). https://doi.org/10.1016/j.wear.2008.12.032

[8] Yang Y L, Shang H F, Pei H P, Xu J M, Liang Y. Role of temperature in tribolayers in fretting wear of γ-TiAl alloy. *Friction* **12**(5): 939-953 (2024). https://doi.org/10.1007/s40544-023-0807-x

[9] Mengis L, Grimme C, Galetz M C. High-temperature sliding wear behavior of an intermetallic γ–based TiAl alloy. *Wear* **426-427**: 341-347 (2019). https://doi.org/10.1016/j.wear.2018.11.025

[10] Yang Y L, Wang C L, Gesang Y Z, Shang H F, Shao T M. Fretting wear evolution of γ-TiAl alloy. *Tribol Int* **154**: 106721 (2021). https://doi.org/10.1016/j.triboint.2020.106721

[11] Hager C H, Sander J, Sharma S, Voevodin A, Segall A. The effect of temperature on gross slip fretting wear of cold-sprayed nickel coatings on Ti6Al4V interfaces. *Tribol Int* **42**: 491-502 (2009). https://doi.org/10.1016/j.triboint.2008.08.009

Just Accepted

[12] Dreano A, Fouvry S, Guillonneau. Understanding and formalization of the fretting-wear behavior of a cobalt-based alloy at high temperature. *Wear* **452-453**: 203297 (2020). https://doi.org/10.1016/j.wear.2020.203297

[13] Dreano A, Fouvry S, and Guillonneau G. A combined friction energy and tribo-oxidation formulation to describe the high temperature fretting wear response of a cobalt-based alloy. *Wear* **426-427**: 712-724 (2019). https://doi.org/10.1016/j.wear.2019.01.023

[14] Hager C H, Hu J, Muratore C, Voevodin A A, Grandhi R. The mechanisms of gross slip fretting wear on nickel oxide/Ti6Al4V mated surfaces. *Wear* **268**: 1195-1204 (2010). https://doi.org/10.1016/j.wear.2009.11.004

[15] Glascott J, Wood G C, Stott F H. The influence of experimental variables on the development and maintenance of wear-protective oxides during sliding of high-temperature iron-base alloys. *Proc IMechE Part J: J Eng Tribol* **199**(13): 35-41 (1985). https://doi.org/10.1243/PIME_PROC_1985_199_088_02

[16] Koricherla M V, Torgerson T B, Alidokht S A. High temperature sliding wear behavior and mechanisms of cold-sprayed Ti and Ti–TiC composite coatings. *Wear* **476**: 203746 (2021). https://doi.org/10.1016/j.wear.2021.203746

[17] Dreano A, Baydoun S, Fouvry S. Influence of a pre-existing glaze layer on the fretting-wear response of HS25 cobalt-based alloy subjected to various temperature conditions. *Wear* **488**: 204144 (2022). https://doi.org/10.1016/j.wear.2021.204144

[18] Fouvry S, Kapsa P, Vincent L. Analysis of sliding behaviour for fretting loadings: determination of transition criteria. *Wear* **185**: 35-46 (1995). https://doi.org/10.1016/0043-1648(94)06582-9

[19] Biesinger M C, Payne B P, Grosvenor A P, Lau L M, Gerson A R. Resolving surface chemical states in XPS analysis of first row transition metals, oxides and hydroxides. *Appl Surf Sci* **257**: 2717-2730 (2011). https://doi.org/10.1016/j.apsusc.2010.10.051

Just Accepted

[20] Jian S Q, Wang Z, Yang Z L, Ma J X, Yang C. Unveiling the reasons for corrosion resistance difference between two phases of the Fe40Cr40Ni20 duplex MEA in the transpassive region. *Corros Sci* **257**:113277 (2025). https://doi.org/10.1016/j.corsci.2025.113277

[21] Kato H, Komai K. Tribofilm formation and mild wear by tribo-sintering of nanometer-sized oxide particles on rubbing steel surfaces. *Wear* **262**: 36-41 (2007). https://doi.org/10.1016/j.wear.2006.03.046

[22] Kirk A M, Shipway P H, Sun W, Bennett C J. Debris development in fretting contacts - debris particles and debris beds. *Tribol Int* **149**: 105592 (2020). https://doi.org/10.1016/j.triboint.2019.01.051

[23] Viat A, Dreano A, Fouvry S, Barros M D, Henne J. Fretting wear of pure cobalt chromium and nickel to identify the distinct roles of HS25 alloying elements in high temperature glaze layer formation. *Wear* **376-377**: 1043-1054 (2017). https://doi.org/10.1016/j.wear.2017.01.049

[24] Jiang J R, Stott F H, Stack M M. The role of triboparticulates in dry sliding wear. *Tribol Int* **31**: 245-256 (1998). https://doi.org/10.1016/S0301-679X(98)00028-0

[25] Kim J I, Jang Y J, Kim J, Jeong J H. Improvement of running-in process of tetrahedral amorphous carbon film sliding against Si_3N_4 under humid air by O_2 plasma post-irradiation. *Appl Surf Sci* **538**: 147957 (2021). https://doi.org/10.1016/j.apsusc.2020.147957

[26] Wang X H, Gan B B, Xu X J, Zha X Q, Zhang X Y. Fretting-corrosion wear of 17-4PH stainless steels subjected to different aging temperature under simulated sulfuric acid rain condition. *Surf Sci Tech* **4**: 54 (2026). https://doi.org/10.1007/s44251-026-00158-0

[27] Bombac D, Gintalas M, Kugler G, Tereclj M. Mechanisms of oxidation degradation of Cr12 roller steel during thermal fatigue tests. *Metals* **10**: 450 (2020). https://doi.org/10.3390/met10040450

[28] Li W, Cao R, Zhu F, Yan Y J, Ma J Y. Damage induced bending strength variation and crack initiation mechanism during thermal cycling shock of laser deposited Stellite alloy coating for engine valve. *J Mater Res Technol* **36**: 6062-6074 (2025). https://doi.org/10.1016/j.jmrt.2025.04.214

Just Accepted

[29] Li C, Du F, Zhu P M, Xu G N, Wei S Y. High temperature wear–fracture coupling mechanisms in YSZ abradable sealing coatings. *Tribol Int* **218**: 111725 (2026). https://doi.org/10.1016/j.triboint.2026.111725

[30] Yang X, Zeng J Y, Zhang H, Wang J S, Sun J B. Correlation between microstructure, chemical components and tribological properties of plasma-sprayed Cr_2O_3-based coatings. *Ceram Int* **44**: 11054-11068 (2018). https://doi.org/10.1016/j.ceramint.2018.03.004

[31] Tripathi D, Dey T K. Effect of particle size distribution on thermo-mechanical properties of NiO filled LDPE composites. *Bull Mater Sci* **42**: 174 (2019). https://doi.org/10.1007/s12034-019-1853-x

[32] Karthikeyan S, Subramani R, Balasubramanian V, Yishak S. Effects of thermal spray processes on the development microstructure and thermal properties of NiCrAlY bond coats deposited over superni C-263 aero engine combustor liner alloy. *Mater Res Express* **12**: 076511, (2025). https://doi.org/10.1088/2053-1591/adebe6

[33] Wang Y J, Jia Z, Ji J J, Lu W J, Liu D X. Tribo-oxidation mechanism of gradient nanostructured Inconel 625 alloy during high-temperature wear. *Wear* **558-559**: 205581 (2024). https://doi.org/10.1016/j.wear.2024.205581

[34] Wang D W, Xu J K, Wang F Y, Zhao Y, Xiang Z Y. A comprehensive review on the fretting wear of electrical contact interface. *Friction* **13**(8): 9441012 (2025). https://doi.org/10.26599/FRICT.2025.9441012

[35] Huang X R, Jing J N, Wang Q, Luo D B, Wang Z W. Evaluation of plasma-sprayed NiCrAlY/Cr3C2/h-BN coatings oxidation behavior on T22 boiler steel alloy. *Surf Sci Tech* **4**: 4 (2026). https://doi.org/10.1007/s44251-026-00132-w

[36] Wang Y J, Zhao X Q, Hao E K, Bu Z Y, An Y L. High temperature induced “glaze” layer formed in HVOF-sprayed NiCrWMoCuCBFe coating and its wear reduction mechanism. *Friction* **10**(9): 1424-1438 (2022). https://doi.org/10.1007/s40544-021-0557-6.

Just Accepted

[37] Zhang C C, New R W. Understanding the role of glaze layer with aligned images from multiple surface characterization techniques. *Wear* **477**: 203837 (2021). https://doi.org/10.1016/j.wear.2021.203837

[38] Pei H P, Yao L P, Yang Y L, Liang Y, Shao T M. Investigation on mechanisms governing tribological behaviors of NiCrFeAl-hBN coating and Ti_2AlNb alloy at elevated temperatures. *Tribol Int* **219**: 111870 (2026). https://doi.org/10.1016/j.triboint.2026.111870

Author biography



Yulei Yang. He received his Ph.D. degree from State Key Laboratory of Tribology, Tsinghua University, in June 2021. He joined Nanjing University of Science and Technology (NJUST) in July 2021. He is an associate Professor in NJUST. His research interests cover fretting wear, surface engineering, and tribology for bearings.



Chunhui Gao，He received his Ph.D. in Mechanics from Beijing Institute of Technology in June 2018. He joined the Beijing Power Machinery Research Institute in 2018 and is currently a senior engineer, primarily focusing on the overall structural design of air-breathing combined cycle propulsion systems, as well as lightweight heat-resistant materials and their application validation.

Just Accepted